









## Article:

Magnetic Clusters in the  $(\text{CuInSe}_2)_{1-x} (\text{TaSe})_x$  Alloy System ( $0 < x \leq 0.5$ )

P. Grima-Gallardo<sup>1,2,3\*</sup> , G.E. Delgado<sup>4</sup> , A. Velásquez<sup>2,3</sup> , L. Nieves<sup>1,2,3</sup> ,  
E. Pérez-C.<sup>5</sup> , A. Rodríguez-R.<sup>6</sup> , J.A. Aitken<sup>7</sup> , D.P. Rai<sup>8</sup> 

<sup>1</sup>Centro de Estudios en Semiconductores, Departamento de Física, Facultad de Ciencias,  
Universidad de Los Andes, Mérida, Venezuela

<sup>2</sup>Centro Nacional de Tecnologías Ópticas, Mérida, Venezuela

<sup>3</sup>Centro de Investigaciones de Astronomía, Mérida, Venezuela

★ See affiliations page 100

Recibido: agosto 2021

Aceptado: noviembre 2021

Autor para correspondencia: P. Grima-G. e-mail: peg1952@gmail.com,

DOI: <https://doi.org/10.5281/zenodo.6427907>

## Abstract

Polycrystalline samples of  $(\text{CuInSe}_2)_{1-x} (\text{TaSe})_x$  system were prepared by the melt and anneal technique in the composition range  $0 < x \leq 0.5$ . It was found that the solubility of TaSe in the  $\text{CuInSe}_2$  ternary matrix is around 10 %; however, up to  $x = 0.5$  are composed by a mean tetragonal  $\text{CuInSe}_2$ -like phase with traces of the  $\text{TaIn}_{0.67}\text{Se}_2$  phase. A preliminary T-x phase diagram is presented. To determinate the induced magnetic behavior, DC magnetic susceptibility measurements as a function of temperature, using the Zero Field Cooling-Field Cooling (ZFC-FC) protocol, were performed in samples with compositions  $x = 0.05$  and  $0.5$ . It was found that the magnetic behavior evolves from diamagnetic ( $\text{CuInSe}_2$ ,  $x = 0$ ) to paramagnetic ( $x = 0.05$ ) to weak ferromagnetic ( $x = 0.5$ ). The observed hysteresis between FC and ZFC curves, for  $x = 0.05$  and  $x = 0.5$  suggest the presence of magnetic clusters; fitting FC curves with Langevin function it was found that clusters are composed for approximately  $10^3$  Ta-atoms.

**Keywords:** semiconductors; alloys; T-x phase diagram; X-ray diffraction; scanning electron microscopy; differential thermal analysis; magnetic susceptibility.

## Artículo:

Conglomerados magnéticos en el sistema de aleaciones  $(\text{CuInSe}_2)_{1-x} (\text{TaSe})_x$  ( $0 < x \leq 0,5$ )

## Resumen

Muestras policristalinas del sistema  $(\text{CuInSe}_2)_{1-x} (\text{TaSe})_x$  fueron preparadas por la técnica de fusión y recocido en el rango de composiciones  $0 < x \leq 0,5$ . Se encontró que la solubilidad del TaSe en la matriz ternaria del  $\text{CuInSe}_2$  es de aproximadamente 10 %; sin embargo, hasta la composición  $x = 0,5$  tienen una fase principal de tipo tetragonal  $\text{CuInSe}_2$  con trazas de la fase  $\text{TaIn}_{0.67}\text{Se}_2$ . Un diagrama de fases T-x preliminar es presentado. Para determinar el comportamiento magnético inducido, las medidas de susceptibilidad magnética DC fueron estimadas en función de la temperatura, usando el protocolo de Enfriamiento Cero Campo-Enfriamiento con Campo (ECC-EC) en las muestras  $x = 0,05$  y  $0,5$ . Se encontró que el comportamiento magnético evoluciona de diamagnético ( $\text{CuInSe}_2$ ,  $x = 0$ ) a paramagnético ( $x = 0,05$ ) y ferromagnético débil ( $x = 0,5$ ). La histéresis observada entre las curvas ECC y EC, para  $x = 0,05$  y  $x = 0,5$ , sugiere la presencia de conglomerados magnéticos; el ajuste de las curvas con la función de Langevin muestra que los conglomerados están compuestos por aproximadamente  $10^3$  átomos de Ta.

**Palabras clave:** semiconductores; aleaciones, diagrama de fases T-x, difracción de rayos-X, microscopía electrónica de barrido, análisis térmico diferencial, susceptibilidad magnética.

## 1 Introduction

CuInSe<sub>2</sub> is an A<sup>I</sup>-B<sup>III</sup>-C<sup>VI</sup><sub>2</sub> semiconductor material which crystallize in the tetragonal chalcopyrite structure, space group  $I\bar{4}2d$  (No122), widely studied because of its applications in the photovoltaic industry [1]–[5]. Moreover, the discovery in the last years of room temperature ferromagnetism (RT-FM) in the analogous A<sup>II</sup>-B<sup>IV</sup>-C<sup>V</sup><sub>2</sub> compounds with transition metals (TM) [6]–[22] has prompted a new and renewed interest in his research. Particularly, the magnetism of CuInSe<sub>2</sub> doped and/or alloyed with Mn, Fe and Ta has been reported before [18, 19, 23, 24] founding paramagnetic, superparamagnetic and spinglass behaviors (see Table 1).

RT-FM arises from the interaction of holes (created by substitution of B<sup>IV</sup> or B<sup>III</sup> cations by TM) with the local moment of the TM *d* electrons [25, 26]; however, it is also argued that it is due by the presence of magnetic secondary phases such as MnP and MnAs [26]–[30]. Kochura *et al.* [27], in samples prepared by solid state reaction under the condition of fast cooling, found that exist three types of magnetic species in A<sup>II</sup>B<sup>IV</sup>C<sup>V</sup><sub>2</sub>; Mn alloys: a) substitution of Mn ions making Mn complexes (especially dimers), b) MnAs micro-precipitates, and c) MnAs nanosize precipitates (clusters with a mean diameter of 3 nm).

Although the origin of RT-FM is still matter of investigation, it is well established that is composition dependent, at low values of *x*, the alloy shows a typical paramagnetic behavior (or also superparamagnetic) [9, 11] whereas for higher values of *x*, a critical *x<sub>c</sub>* value is attained for which, the paramagnetic to ferromagnetic transition occurs. It is also worth to note that *T<sub>c</sub>* values are approximately the same for all A<sup>II</sup>B<sup>IV</sup>C<sup>V</sup><sub>2</sub>/Mn alloys suggesting that this transition is related to Mn-based secondary phases more than substitution of cations for Mn<sup>2+</sup> in the ternary matrix.

It is interesting to compare theoretical calculations with experimental results. Katamani *et al.* [31, 32], using KKR-CPA-LDA method, predict that ferromagnetic states are stable in (Cd<sub>1-x</sub>V<sub>x</sub>)GeP<sub>2</sub> and (Cd<sub>1-x</sub>Cr<sub>x</sub>)GeP<sub>2</sub> alloys, whereas (Cd<sub>1-x</sub>Mn<sub>x</sub>)GeP<sub>2</sub>, (Cd<sub>1-x</sub>Fe<sub>x</sub>)GeP<sub>2</sub> and (Cd<sub>1-x</sub>Co<sub>x</sub>)GeP<sub>2</sub> must show spinglass-like ground

states (calculations were made using *x* = 0.1). They also found that Ti and Ni substitutions in CdGeP<sub>2</sub> could not have a net magnetic moment (the same are applicable to ZnGeP<sub>2</sub> and CdSiAs<sub>2</sub>). On the other hand, the ferromagnetic state was found to be stable in AgGaS<sub>2</sub> (CuAlS<sub>2</sub>) doped with Ti, V, Cr and Mn, whereas doping with Fe, Co and Ni must stabilizes a spinglass-like state. The work of Zhao *et al.* [25], using first principle calculations, coincides with Katamani and predicts that Mn doping at the III site in A<sup>I</sup>B<sup>III</sup>C<sup>VI</sup><sub>2</sub> compounds provides holes that must stabilize ferromagnetic coupling between Mn ions. The predictions of both works (Katamani and Zhao) are contradictory that which has been observed experimentally. The reason for the discrepancies between theoretical expectations and experimental results is not clear until now. It has been suggested that stabilization of ferromagnetism is also due to the interaction of holes with Mn magnetic moments induced by:

- Intrinsic defects [33, 34];
- Non-uniform spatial distribution of carriers and/or and magnetic ions [35]; or
- Nanoscale phase separation, driven either by randomness in the carrier and spin subsystems or by limited solubility of transition metals in the host semiconductor, which leads to spinodal decomposition into regions with a small and a large concentration of the magnetic constituents [35].

It is evident that additional experimental work, in greater variety of systems and with larger concentration of the transition metal dopant, is necessary.

This work reports the preparation and characterization of the (CuInSe<sub>2</sub>)<sub>1-x</sub> (TaSe)<sub>x</sub> solid solutions system in the composition range 0 < *x* ≤ 0.5, as a part of the systematic research in A<sup>I</sup>-B<sup>III</sup>-C<sup>VI</sup><sub>2</sub> alloys with TM. Some partial results had been previously reported: XRD diffraction and DTA were presented as short note in a conference [36], for sample *x* = 0.5 (nominally CuTaInSe<sub>3</sub>) the preparation and crystal structure [37, 38] and for sample *x* = 0.25 the magnetic susceptibility [39]. In addition, more exhaustive analysis were added

Table 1: CuInSe<sub>2</sub>: TM alloys previously reported in the literature

Alloys	Magnetic element composition	Synthesis method	Magnetic behavior	$T_c$ [K]	Reference
Cu <sub>1-x</sub> Mn <sub>x</sub> InSe <sub>2</sub>	$0 < x < 0.2$	SSR	PM	—	Yao <i>et al.</i> [18]
CuIn <sub>1-x</sub> Mn <sub>x</sub> Se <sub>2</sub>	$0.0125 < x < 0.2$	SSR	PM	—	Yao <i>et al.</i> [19]
Cu <sub>1-y</sub> In <sub>1-y</sub> Mn <sub>2y</sub> Se <sub>2</sub>	$0.0125 < y < 0.6$	SSR	SPM	—	Torres <i>et al.</i> [23]
(CuIn) <sub>1-x</sub> Fe <sub>x</sub> Se <sub>2-x</sub>	$x = 0.5$	SSR	SG	50	Grima <i>et al.</i> [24]

on XRD diffraction, identification of the phases by SEM measurements, a preliminary T-x phase diagram, and DC magnetic susceptibility measurements for samples  $x = 0.05$  and  $x = 0.5$ .

## 2 Experimental Procedure

### 2.1 Samples Synthesis

Polycrystalline samples with a weight of approximately 1 g each, belonging to the (CuInSe<sub>2</sub>)<sub>1-x</sub>(TaSe)<sub>x</sub> solid solutions system were prepared using the melt and anneal technique, in steps of  $x = 0.1$  in the composition range  $0 < x \leq 0.5$ , and in addition samples  $x = 0.05$  and  $0.25$  were also prepared. Starting materials (Cu, In, Ta, and Se) with a nominal purity of (at least) 99.99 wt. % in the stoichiometric ratio were mixed together in an evacuated ( $10^{-4}$  Torr) and sealed quartz tube with the inner walls previously carbonized in order to prevent chemical reaction of the elements with quartz. The quartz ampoule was heated until 493 K (melting point of Se) keeping this temperature for 48 h, shaking all the time by means of a electromechanical motor. This procedure guarantees the formation of binary species at low temperature and avoids the existence of Se free gas at high temperature, which could produce explosions or Se deficiency in the ingot. Then the temperature was slowly increased until 1423 K (maximal recommended work temperature of the furnace) with the mechanical shaker always connected for a better mix of the components. After 24 h, the mechanical shaker was disconnected and the cooling cycle begins until the anneal temperature (800 K). Then, the ampoule was keeping at the annealing temperature during 1 month, in order to obtain the thermal equilibrium

of the atoms in the sample. Finally, the furnace was switching off.

### 2.2 Scanning Electron Microscopy (SEM)

The stoichiometric relation of the samples was investigated by scanning electron microscopy (SEM) technique, using *Hitachi S2500* equipment. The micro chemical composition was found by an energy-dispersive x-ray spectrometer (EDS) coupled with a computer-based multichannel analyzer (MCA), (*Delta III* analysis and *Quantex* software, *Keve*). For the EDS analysis,  $K_{\alpha}$  lines were used. Accelerating voltage was 15 kV. The samples were tilted 35 degrees. A standarless EDS analysis was made with a relative error of 5 to 10 % and detection limits of the order of 0.3 wt. %, where the k-ratios are based on theoretical standards.

### 2.3 X-Ray Diffraction (XRD)

X-ray powder diffraction data was collected by means of a diffractometer (*Bruker D5005*) equipped with a graphite monochromator ( $\text{CuK}_{\alpha} = 1.54059 \text{ \AA}$ ) at 40 kV and 20 mA. Silicon powder was used as an external standard. The samples were scanned from  $10 - 100^{\circ} 2\theta$ , with a step size of  $0.02^{\circ}$  and counting time of 20 s. The Bruker analytical software was used to establish the positions of the peaks from the  $\text{CuK}_{\alpha_1}$  component and to strip mathematically the  $\text{CuK}_{\alpha_2}$  components from each reflection. The peak positions were extracted by means of single-peak profile fitting carried out through the *Bruker DIFFRAC*<sup>plus</sup> software. Each reflection was modeled by means of a pseudo-Voigt function.

## 2.4 Differential Thermal Analysis (DTA)

Differential Thermal Analysis (DTA) measurements were carried out in a fully automatic *Perkin-Elmer* apparatus, which consists in a *Khantal* resistance furnace ( $T_{max} = 1650$  K) equipped with Pt/Pt-Rh thermocouples and an informatics system for the automatic acquisition data. The internal standard used was a high purity (99.99 wt. %) piece of gold. The temperature runs have been performed from ambient temperature to 1400–1500 K, which is the recommended operative limit. The heating rate was controlled electronically to  $20 \text{ K h}^{-1}$ ; the cooling rate was given by the natural cooling of the furnace after switching off. From the thermogram, transition temperatures were manually obtained from the  $\Delta T$  vs.  $T$  graph with the criteria that the transition occurs at the intersection of the baseline with the slope of the thermal transition peak, as usual. The maximum error committed in the determination of transition temperatures by this method was estimated to be  $\pm 10$  K.

## Magnetic Susceptibility

DC magnetic susceptibility measurements as a function of temperature,  $\chi(T)$ , were performed on a *Quantum Design SQUID* magnetometer, equipped with a superconducting magnet able to produce fields up to 5 T. The samples in the form of powder were compacted with a piece of cotton inside the sample holder in order to prevent any movement. Zero-field-cooling and field cooling (ZFC-FC) measurements were carried out in the temperature range of 2 – 300 K.

## 3 Analysis and Discussion

Stoichiometric relations of all the samples were checked out in a thin slide ( $\sim 1$  mm thick) cut off from the center of the ingot. The results are shown in Table 2. The experimental error is estimated in the first decimal place about (0.01). The sum of the percentages does not always add exactly 100 % by approximations of decimals.

General observations are:

- Deviations in the stoichiometry for Cu and Se, in average, lies inside of the estimated experimental error approximately (10 %).
- In the case of In and Ta, deviations (always in average) are higher than the experimental error (20 and 30 %, respectively).
- In average, the quantity of Ta in the samples does not exceed 10 %, suggesting that this is the limit of solid solubility.

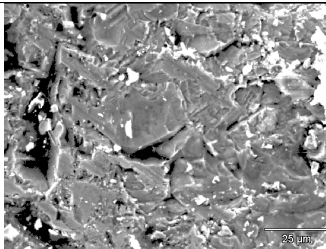
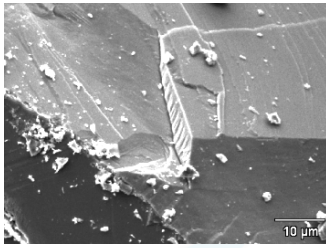
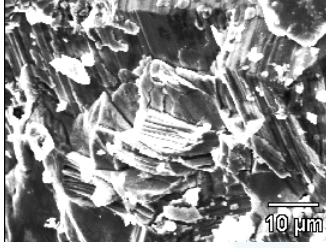
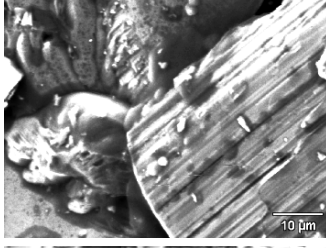
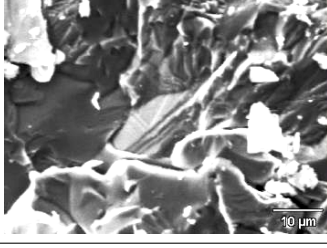
In particular, in sample  $x = 0.1$ , Cu stoichiometry is close to nominal, whereas In and Ta are somewhat low. For sample  $x = 0.2$ , three experiences give a similar behavior to sample  $x = 0.1$  but two experiments (2 and 3) give lower stoichiometry values for Cu and In and higher for Ta with respect to nominal. Behavior of sample  $x = 0.3$  is similar to sample  $x = 0.2$ . For samples  $x = 0.1$ , 0.2 and 0.3, although the nominal stoichiometry values of Cu and In are the same, the experimental values of Cu are always higher than In; this behavior is inverted for sample  $x = 0.4$ . Sample  $x = 0.5$  have a similar behavior of samples  $x = 0.1$ , 0.2 and 0.3 with respect to the relation between Cu and In, but the Ta values are too lower with respect to nominal, with exception of experiment (Exp. 1) where the value of Ta is higher than nominal but of Cu and In are lower; which can be seen in Table 2.

Concerning the distribution of Cu, In Ta and Se atoms in the samples, it can be observed in Figure 1 that it is quite homogenous (Cu: red, Se: yellow, Indium: blue, Tantalum: green) indicative that the observations about variations in the stoichiometry are more due to local fluctuations and not too large regions of different phases. Effectively, in SEM technique the usual resolution is in the order of one digit in nanometer units (although in some sophisticated equipment it can be obtained resolutions of 0.4 nm see *Hitachi Launches World's Highest Resolution FE-SEM*, in *Nanotech Now* <<http://www.nanotech-now.com/>>), that is around  $10^{-4}$  times the size of the white trait scale (10 to 25  $\mu\text{m}$ ) in Figure 1.

However, under a more exhaustive examination, for sample  $x=1/3$ , Figure 2 show little structures



Table 2: Microphotographs and measured stoichiometry for  $(\text{CuInSe}_2)_{1-x} (\text{TaSe})_x$  alloys with  $x = 0.1, 0.2, 0.3, 0.4$  and  $0.5$  (in red color the nominal stoichiometry)

Microphotographs	Nominal composition, experiment (Exp.)	Cu at %	In at %	Se at %	Ta at %
	$x = 0.1$	<b>23.7</b>	<b>23.7</b>	<b>50.0</b>	<b>2.6</b>
	Exp. 1	22.7	17.7	58.8	0.8
	Exp. 2	21.7	18.1	59.4	0.8
	Exp. 3	22.1	18.4	58.3	1.2
	Exp. 4	21.1	16.7	60.4	1.7
	Exp. 5	21.9	17.8	59.2	1.2
	$x = 0.2$	<b>22.2</b>	<b>22.2</b>	<b>50.0</b>	<b>5.6</b>
	Exp. 1	20.2	18.1	59.1	2.5
	Exp. 2	16.4	13.5	61.1	9.0
	Exp. 3	16.4	12.5	62.1	9.0
	Exp. 4	20.1	16.1	60.7	3.1
	Exp. 5	20.2	17.1	59.9	2.8
	$x = 0.3$	<b>20.6</b>	<b>20.6</b>	<b>50.0</b>	<b>8.8</b>
	Exp. 1	16.8	12.5	60.2	10.5
	Exp. 2	14.8	11.9	61.0	12.3
	Exp. 3	22.3	15.6	53.2	8.7
	Exp. 4	28.7	17.3	55.6	6.4
	Exp. 5	20.7	14.4	57.5	9.5
	$x = 0.4$	<b>18.8</b>	<b>18.8</b>	<b>50.0</b>	<b>12.5</b>
	Exp. 1	12.5	19.5	54.6	12.5
	Exp. 2	16.8	18.6	57.3	7.3
	Exp. 3	17.3	20.1	57.6	5.0
	Exp. 4	18.8	21.1	58.0	2.1
	Exp. 5	16.7	19.8	56.9	6.7
	$x = 0.5$	<b>16.7</b>	<b>16.7</b>	<b>50.0</b>	<b>16.7</b>
	Exp. 1	11.8	3.6	65.6	19.1
	Exp. 2	18.8	14.3	59.0	7.9
	Exp. 3	21.3	13.2	61.3	4.3
	Exp. 4	22.3	16.0	59.7	2.1
	Exp. 5	20.8	14.5	60.1	4.6

with hexagonal symmetry which are identified as  $\text{TaIn}_{0.67}\text{Se}_2$  as a secondary phase.

$\text{TaIn}_{0.67}\text{Se}_2$  was a previously reported compound [40] which crystallizes in the hexagonal structure, space group  $P\bar{6}m2$  (N 187), with

cell parameters  $a = b = 3.45 \text{ \AA}$ ,  $c = 8.22 \text{ \AA}$ ,  $\alpha = \beta = 90^\circ$ ,  $\gamma = 120^\circ$ . The nominal stoichiometry for  $\text{TaIn}_{0.67}\text{Se}_2$  is Ta: 27.25 %, In: 18.26 %, and Se: 54.50 % which is very close to those observed in points 1, 3, 4, and 5 (Figure 2(a) microphotography,

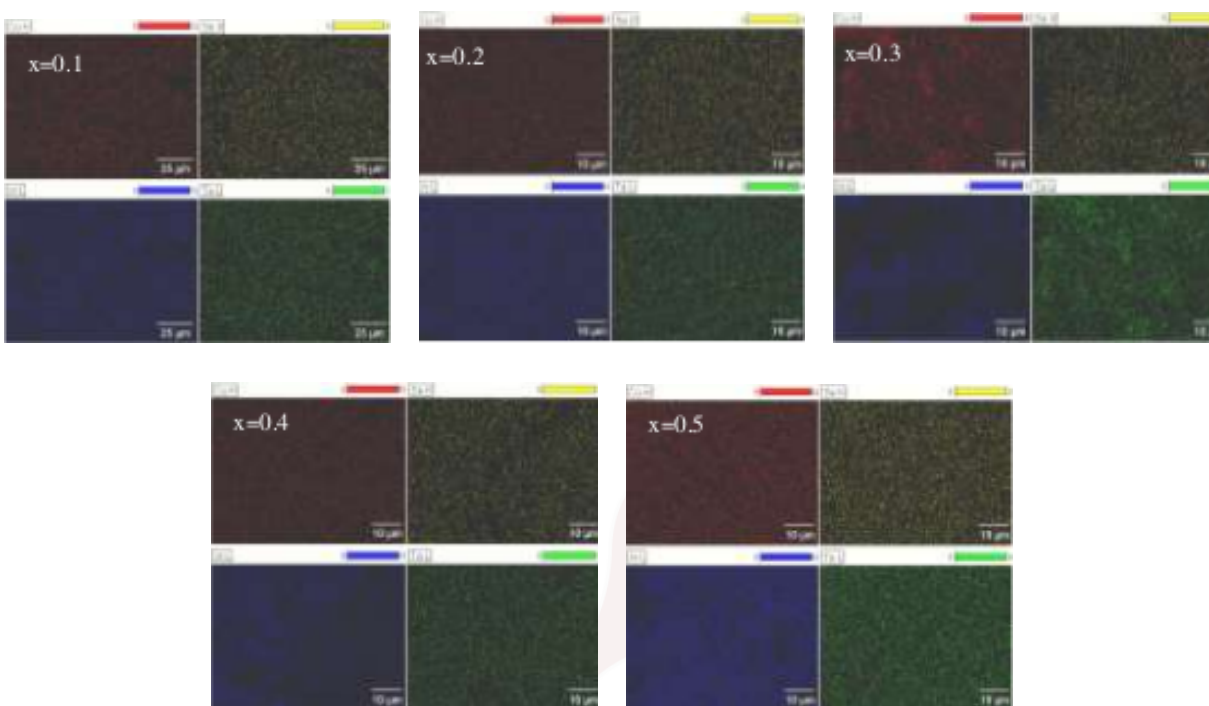


Figure 1: Distribution of Cu, Se, In and Ta in the samples  $x = 0.1, 0.2, 0.3, 0.4$  and  $0.5$

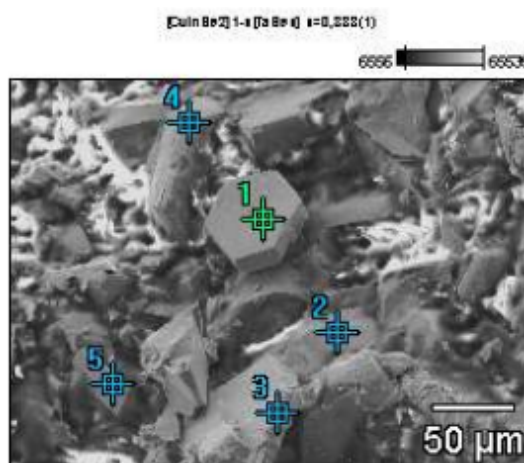
Table 3: Comparison of the experimental stoichiometry of sample  $x = 1/3$  with the nominal stoichiometry of  $\text{TaIn}_{0.67}\text{Se}_2$  (in red)

[CuInSe <sub>2</sub> ] <sub>1-x</sub> [TaSe <sub>x</sub> ] Microphotography 1					
		Cu	Se	In	Ta
Simple $x = 0, 333$	Exp 1	0.20 (—)	63.72 (54.5)	14.77 (18.3)	21.31 (27.3)
	Exp 3	1.38	61.51	16.44	20.67
	Exp 4	0.13	64.91	14.34	20.62
	Exp 5	1.33	64.81	13.55	20.31
[CuInSe <sub>2</sub> ] <sub>1-x</sub> [TaSe <sub>x</sub> ] Microphotography 2					
		Cu	Se	In	Ta
Simple $x = 0, 333$	Exp 1	0.61 (—)	63.78 (54.5)	13.89 (18.3)	21.72 (27.3)
	Exp 2	1.36	63.27	14.54	20.82
	Exp 3	2.07	65.16	11.56	21.21
	Exp 5	0.70	63.31	15.21	20.77

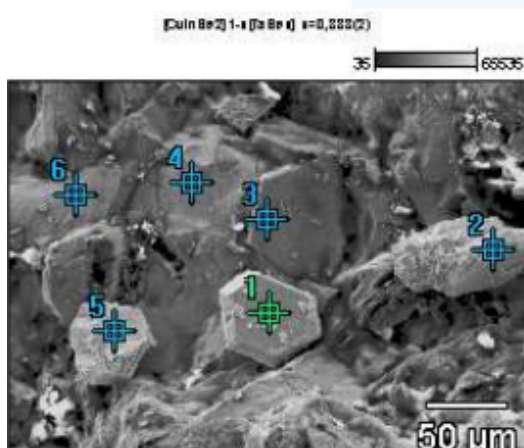
upper Table 3) and 1, 2, 3, and 5 (Figure 2(b) microphotography, bottom Table 3).

The lattice parameters of  $(\text{CuInSe}_2)_{1-x}(\text{TaSe})_x$  solid solutions were previously reported [37] (Figure 3). It can be observed that parameters  $a$  and  $c$  remain nearly constant in the entire composition range studied. However, it is worth a short discussion about the covalent radii of Cu, Ta, and In (Table 4) and the occupancy of the

Ta atoms in the  $\text{CuInSe}_2$  matrix. Although there is considerable dispersion about the covalent radius values from different authors, it is well established that it increases from left to right and from upper to bottom in the periodic table: Cu has the lower value whereas Ta and In are similar. The fact that the lattice parameters do not change with composition in  $(\text{CuInSe}_2)_{1-x}(\text{TaSe})_x$  solid solutions up to  $x = 0.5$  suggests that Ta preferably substitutes In in the  $\text{CuInSe}_2$  matrix. That may be the reason



(a)



(b)

Figure 2: Microphotographs of sample  $x=1/3$ 

for which the observed general trend of deviation in stoichiometry for the nominal values is higher in In than in Cu.

Figure 4 display the diffraction patterns of compositions  $x = 0.1, 0.2$ , and  $0.5$ , which have not been shown in a previous report [37]. In Figure 4:

- The experimental diffraction patterns are displayed in black.
- A calculated diffraction pattern of  $\text{CuInSe}_2$ , using Power Cell software <http://www.ccp14.ac.uk/ccp/web-mirrors/powdcell/> in red.
- Green ticks denote the stronger peaks of  $\text{TaIn}_{0.67}\text{Se}_2$  phase which was also observed in SEM measurements.

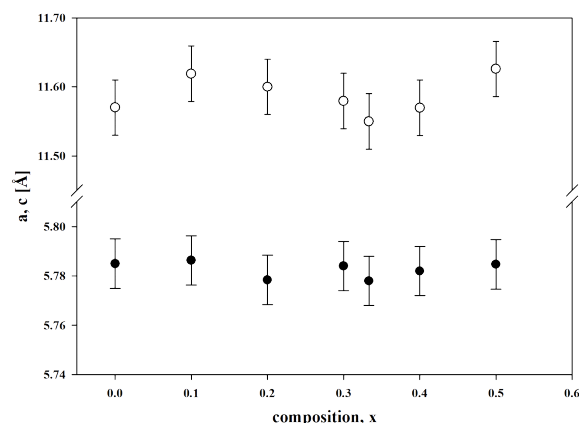


Figure 3: Lattice parameters of  $(\text{CuInSe}_2)_{1-x}(\text{TaSe})_x$  alloys; white circles: parameter  $c$ , black circles parameter  $a$

Table 4: Values of the covalent radii for Cu, In, and Ta

Cation	Covalent radius [Å]				
	Source				
	1	2	3	4	5
<b>Cu</b>	1.17	1.38	1.38	1.17	1.12
<b>In</b>	1.44	1.44	1.44	1.50	1.42
<b>Ta</b>	1.34	1.38	1.45	1.34	1.46

Source 1: Periodic – Covalente radius at

<https://EnvironmentalChemistry.com/>

Source 2: Periodic – Covalent radius at

<https://EnvironmentalChemistry.com/>

Source 3: Crystallmaker – Atomic radii at

<http://www.crystallmaker.com/>

Source4: Covalent radius table at

<http://chemistry-reference.com/>

Source 5: Figure 1 in Pyykkö and Atsumi [41].

- Asterisks denotes not identified peaks.

The coincidence of the  $\text{CuInSe}_2$  peaks with those of the alloys ( $x = 0.1, 0.2$ , and  $0.5$ ) confirms that the lattice parameters remain constant in the entire composition range studied. The mean difference between diffraction patterns results in peak intensities.

The intensities of the diffraction peaks are related to the occupation of the crystallographic sites by cations; however, Ta will replace no way of knowing, a priori, which cation, Cu or In. Moreover,

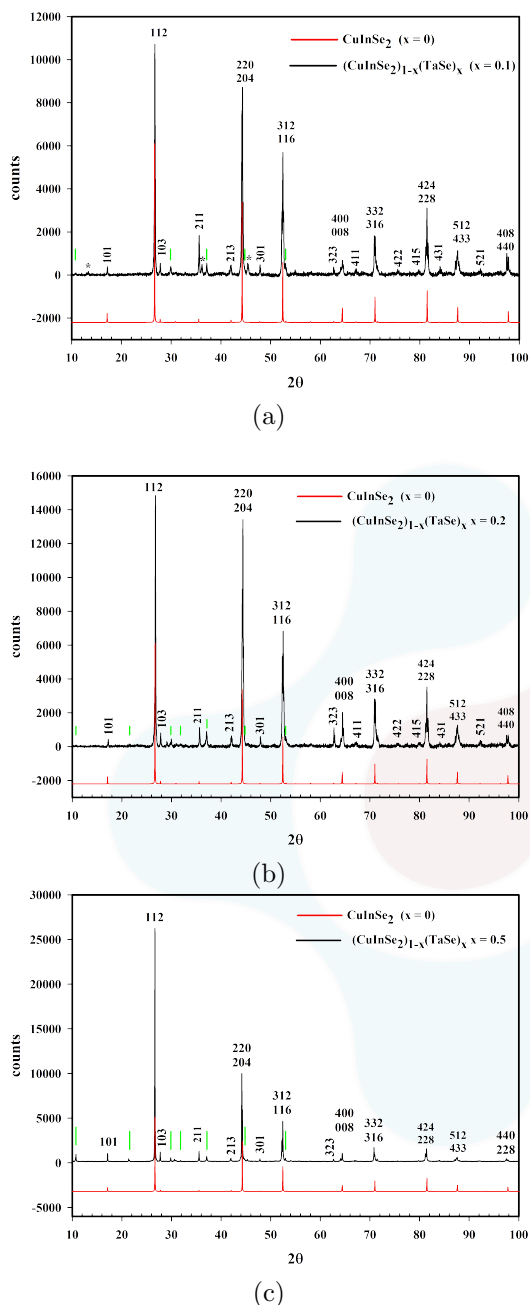


Figure 4: XRD patterns for samples  $x = 0.1$  (a),  $x = 0.2$  (b) and  $x = 0.5$  (c). In red:  $\text{CuInSe}_2$  calculated diffraction pattern using Powder Cell software <http://www.ccp14.ac.uk/>. Green ticks denote the positions of the stronger peaks for  $\text{TaIn}_{0.67}\text{Se}_2$  phase. Asterisks signal not identified peaks

refinements using Rietveld method suggest that at least one crystallographic site is occupied at random

for the three cations, as is the case of  $\text{CuTaInSe}_3$ , the sample  $x = 0.5$  [24].

Concerning this sample ( $x = 0.5$ ), it can be observed in Figure 3 that the relation between the intensities of the two stronger peaks ( $I_{112}/I_{220}$ ) is 2.62, whereas for samples  $x = 0$ ,  $x = 0.1$ , and  $x = 0.2$  the values are 1.53, 1.22, and 1.10, respectively. In previous works on chalcopyrite/metal transition alloys, it was extensively discussed that the ordered chalcopyrite structure, space group  $I\bar{4}2d$  (N 122) evolves with composition to a semi-ordered chalcopyrite-like structure,  $P\bar{4}2c$  (N 122) until a new cationic rearrangement occurs towards stannite-type structure, space group  $I\bar{4}2m$  (N 121), at  $x = 2/3$  [42, 43].

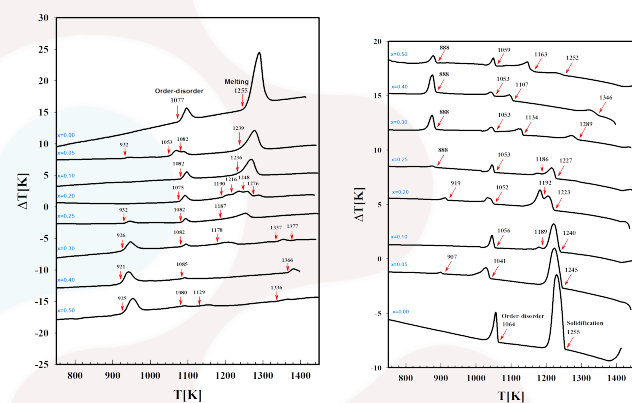


Figure 5: DTA thermograms for  $(\text{CuInSe}_2)_{1-x}(\text{TaSe})_x$  alloys,  $0 \leq x \leq 0.5$ . Left: heating cycle. Right: Cooling cycle

To build a preliminary T-x phase diagram, based on the information obtained by SEM, XRD, and DTA measurements, in Figure 5, DTA thermograms are shown. In heating and cooling cycles, a chalcopyrite-like behavior can be observed. Two transitions, one due to cationic sublattice disorder and another due to melting (or solidification), in the composition interval  $0 \leq x \leq 1$ , although sample  $x = 0.05$  show a little structure at 932 K in the heating (907 in the cooling), suggesting that this is the existing field of the ordered chalcopyrite-like ( $\alpha$ ) phase. For  $x > 0.1$ , the thermogram shows the evolution to another phase with several thermal transitions. Figure 6 shows the proposed T-x phase diagram.



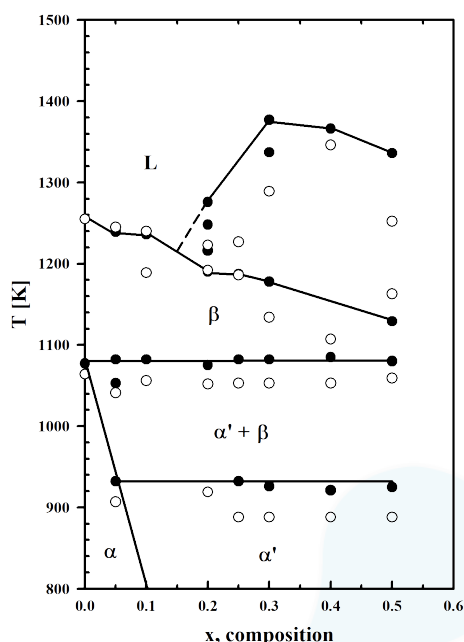


Figure 6: T-x phase diagram for  $(\text{CuInSe}_2)_{1-x}(\text{TaSe})_x$  alloys,  $0 \leq x \leq 0.5$ . Black circles: heating cycle. White circles: cooling cycle.  $\alpha$ : ordered chalcopyrite-like phase;  $\alpha'$ : semi-ordered chalcopyrite phase;  $\beta$ : disordered zincblende phase; L: liquid phase.

The chalcopyrite-like ( $\alpha'$ ) phase field is limited to composition range  $0 \leq x \leq 0.1$  at  $T = 800$  K; with increasing temperature the phase-field decreases until the temperature of  $T = 1077$  K. The semi-ordered ( $\alpha'$ ) phase exist for compositions  $x > 0.1$ , at  $T = 800$  K until  $T = 932$  K whereas, between  $T = 932$  K and  $T = 1077$  K, the  $\alpha'$  phase coexist with the  $\beta$  phase. At  $x=0$ , exists between  $T = 1077$  K and the melting point at 1255 K. The melting point decreases between  $x = 0$  to approximately  $x = 0.15$ , then increases until  $x = 0.3$  and decreases again until  $x = 0.5$ . There is a wide liquid + solid region between  $x = 0.15$  and  $x = 0.5$  but region phases cannot be identified.

Overcooling in the samples is also observed: the thermal transitions in the cooling cycle are observed at a lower temperature than in the heating cycle.

DC magnetic susceptibility measurements were performed in samples  $x=0.05$  and  $1/2$  using SQUID technique and the ZFC-FC protocol (see Figure 7).

Sample  $x = 0.05$  shows a paramagnetic-like behavior with hysteresis between ZFC and FC

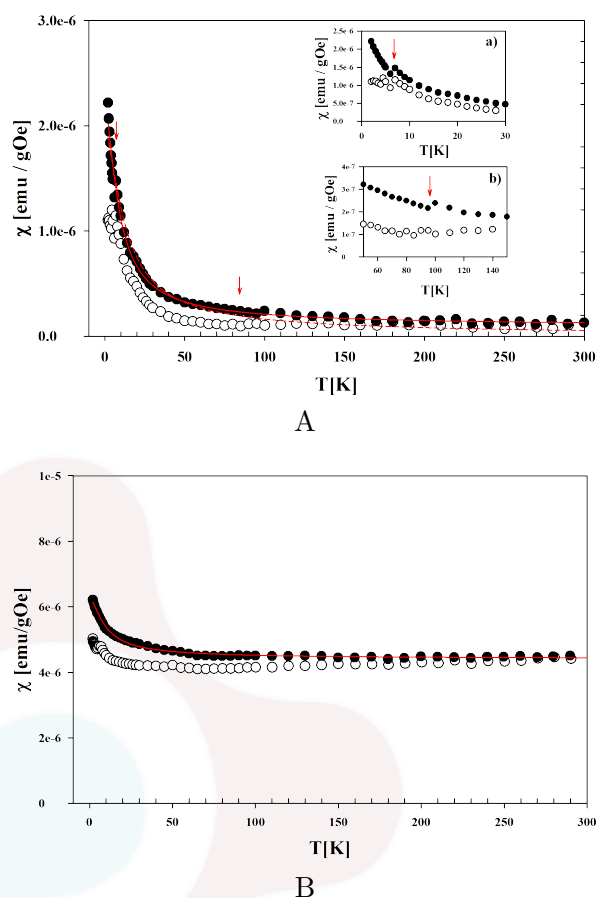


Figure 7: DC mass magnetic susceptibility. A: samples  $x = 0.05$  (A) and B:  $x = 1/2$  belonging to the  $(\text{CuInSe}_2)_{1-x}(\text{TaSe})_x$  solid solutions. ZFC: white circles; ZC. Black circles. Red lines: fit with a Langevin function. The insets in figure A are amplifications at different scales (see red arrows and explanation in the text).

curves typical of systems with magnetic clusters. The position of two little peaks in the FC curve are signaled by red arrows and amplified in the insets. The origin of these two little peaks cannot be explained unambiguously at this stage of this study; however, a possibility is that it can be related to the blocking-unblocking process of magnetic clusters.

Effectively, the peak at lower temperature coincides with a relative maximum of the magnetic susceptibility in the ZFC curve which is typical of systems with a size distribution of the magnetic clusters; this relative maximum in the ZFC curve sometimes also produce a peak in the FC curve as it observed in measurement. For the little structure

Table 5: Results of the fits for sample  $x = 0.05$  (Figure 6)

Equations	$\mu_m/[\mu_B]$	$\chi_0$ [emu/gOe]	$\chi_p$ [emu/gOe]	$R^2$
$\chi = \chi_0 L(x)$	$3.6 \times 10^3$	$2.1 \times 10^{-6}$	—	0.979
$\chi = \chi_0 L(x) + \chi_p$	$2.4 \times 10^3$	$2.2 \times 10^{-6}$	$8.9 \times 10^{-9}$	0.993

at the higher temperature, it is observed only in the FC curve and it is very weak, in consequence, their origin remains speculative.

Two fits (dashed and continuous red lines) were performed on the FC curve; the first one (dashed line) with a simple Langevin function  $\chi(T) = \chi_0 L(x)$  where  $x = \mu H/k_B T$ , being  $\mu$  the mean magnetic moment of the magnetic clusters,  $H$  the applied magnetic field (100 Oe in this experiment),  $k_B$  the Boltzmann constant and  $T$  the absolute temperature. It can be observed that this fit is not good for  $T > 100$  K. For the second fit (continuous red line), a constant term ( $\chi_p$ ) has been added to the Langevin function, suggesting the presence of a little magnetic component that can be due to the presence of the  $\text{TaIn}_{0.67}\text{Se}_2$  secondary phase. This time the fit is better (Table 5). The obtained values for the mean magnetic moment show that clusters are composed of about  $10^3$  Ta atoms.

## 4 Conclusions

$(\text{CuInSe}_2)_{1-x}(\text{TaSe})_x$  solid solutions in the composition range  $0 < x \leq 0.5$  have been investigated. XRD shows a tetragonal chalcopyrite-like phase with lattice parameters very close to  $\text{CuInSe}_2$  and the presence of a secondary phase identified as  $\text{TaIn}_{0.67}\text{Se}_2$  that does not belong to the  $\text{CuInSe}_2$ - $\text{TaSe}$  tie line. The analysis of SEM-EDX shows stoichiometric deviations in Cu and Se elements in the order of the experimental error approximately (10 %) for this technique whereas for In and Ta deviations are, on average, of 23.5 and 34 %; also, always in average, the contents of Ta in the samples never exceed 10 % suggesting than this is the solubility limit. This result coincides with DTA and the obtained preliminary T-x phase diagram. As the amount of Ta increases in the samples, the magnetic behavior evolves from paramagnetic to

weak ferromagnetic. From the fit of magnetic susceptibility measurements with Langevin function, it was found the presence of magnetic nanoclusters which contains around  $10^3$  Ta atoms. For the sample with composition  $x = 0.5$ ,  $T_c > 300$  K; which is the first time, according literature review previously carried out, that room temperature ferromagnetism is observed in I-III-VI<sub>2</sub>/TM alloys.

## Acknowledgments

P. Grima-Gallardo wants to thanks to Dr. Dwight R. Acosta Najarro, Departamento Materia Condensada, Instituto de Física de la Universidad Autónoma de México (UNAM) for SEM-EDX measurements.

## Funding

The authors declare that the financing of this project is by their own income and by the projects of *Centro de Investigaciones de Astronomía, Mérida, Venezuela*.

## Interests conflict

The authors of this work declare that they have no conflict of interest in its publication.

## References

- [1] J.L. Shay and J.H. Wernick. *Ternary Chalcopyrite Semiconductors: Growth, Electronic Properties, and Applications*. Pergamon Press, Oxford, UK, 1974.
- [2] O Madelung. *Semiconductors Data Handbook*. Springer, Berlin, 2004.

- [3] J.L. Shay and S. Wagner. Efficient CuInSe<sub>2</sub>/CdS Solar Cells. *Applied Physics Letters*, 27(2):89–90, 1975.
- [4] L. Stolt and J. Hedström. ZnO/CdS/CuInSe<sub>2</sub> Thin-film Solar Cells with Improved Performance. *Applied Physics Letters*, 62(6):597–599, 1993.
- [5] D. Cahen. Defect Chemical Explanation for the Effect of Air Anneal on CdS/CuInSe<sub>2</sub> Solar Cell Performance. *Applied Physics Letters*, 54(6):558–560, 1989.
- [6] G.A. Medvedkin, T. Ishibashi, T. Nishi, K. Hayata, Y. Hasegawa, and K. Sato. Room Temperature Ferromagnetism in Novel Diluted Magnetic Semiconductor Cd<sub>1-x</sub>Mn<sub>x</sub>GeP<sub>2</sub>. *Japanese Journal of Applied Physics*, 39(Part 2, No. 10A):L949–L951, 2000.
- [7] S. Cho, S. Choi, G.-B. Cha, S.C. Hong, Y. Kim, Y.-J. Zhao, A.J. Freeman, J.B. Ketterson, B.J. Kim, Y.C. Kim, and B.-C. Choi. Room-Temperature Ferromagnetism in (Zn<sub>1-x</sub>Mn<sub>x</sub>)GeP<sub>2</sub> Semiconductors. *Physical Review Letters*, 88(25):257203, 2002.
- [8] S. Choi, J. Choi, S.C. Hong, S. Cho, Y. Kim, and J.B. Ketterson. Mn-doped ZnGeAs<sub>2</sub> and ZnSnAs<sub>2</sub> Single Crystals: Growth, Electrical, and Magnetic Properties. *Journal of the Korean Physical Society*, 42(SPEC. Event: Proceedings of The 11th Seoul International Symposium of the Physics Semiconductors and Applications 2002 - Cheju Island, Korea):S739–S741, 2003.
- [9] R.V. Demin, L.I. Koroleva, S.F. Marenkin, S. Mikhailov, T. Aminov, H. Szymczak, R. Szymczak, and M. Baran. Room-Temperature Ferromagnetism in Mn-doped CdGeAs<sub>2</sub> Chalcopyrite. *Journal of Magnetism and Magnetic Materials*, 290–291(Part 2):1379–1382, 2005.
- [10] L.I. Koroleva, V.Yu. Pavlov, D.M. Zashchirinskiĭ, S.F. Marenkin, S.A. Varnavskii, R. Szymczak, V. Dobrovolskiĭ, and L. Killinskiĭ. Magnetic and Electrical Properties of the ZnGeAs<sub>2</sub> Mn Chalcopyrite. *Physics of the Solid State*, 49:2121–2125, 2007.
- [11] L.I. Koroleva, D.M. Zashchirinskiĭ, T.M. Khapaeva, S.F. Marenkin, I.V. Fedorchenko, R. Szymczak, B. Krzumanska, V. Dobrovolskiĭ, and L. Killinskiĭ. Manganese-Doped ZnSiAs<sub>2</sub> Chalcopyrite: A New Advanced Material for Spintronics. *Physics of the Solid State*, 51(2):303–308, 2009.
- [12] L. Kilanski, M. Gorska, V. Domukhovski, W. Dobrowolski, J.R. Anderson, C.R. Rotundu, S.A. Varniavskii, and S.F. Marenkin. Zn<sub>(1-x)</sub>(Mn,Co)<sub>x</sub>GeAs<sub>2</sub> Ferromagnetic Semiconductor: Magnetic and Transport Properties. *Acta Physica Polonica A*, 114(5):1151–1157, 2008.
- [13] A.V. Kochura, R. Laiho, A. Lashkul, E. Lähderanta, M.S. Shakhov, I.S. Zakharov, S.F. Marenkin, A.V. Molchanov, S.G. Mikhailov, and G.S. Jurev. Synthesis and Magnetic Properties of Mn-doped Cd<sub>0.1</sub>Zn<sub>0.9</sub>GeAs<sub>2</sub> Solid Solutions. *Journal of Physics: Condensed Matter*, 20(33):(335220)1–5, 2008.
- [14] L.-J. Lin, N. Tabatabaie, J.H. Wernick, G.W. Hull, and B. Meagher. Optical, Electronic and Magnetic Semiconductor Mn:CuInTe<sub>2</sub>. *Journal of Electronic Materials*, 17:321–324, 1988.
- [15] P.M. Shand, P.A. Polstra, I. Miotkowski, and B.C. Crooker. Magnetic Behavior of (CuIn)<sub>1-x</sub>Mn<sub>2x</sub>Te<sub>2</sub>. *Journal of Applied Physics*, 75(10):5731–5733, 1994.
- [16] N. Tsuji, H. Kitazawa, and G. Kido. Electric and Magnetic Properties of Mn- and Fe-doped CuInS<sub>2</sub> Compounds. *Physica Status Solidi (a)*, 189(3):951–954, 2002.
- [17] J. Yao, B.W. Rudyk, C.D. Brunetta, K.B. Knorr, H.A. Figure, A. Mar, and J.A. Aitken. Mn Incorporation in CuInS<sub>2</sub> Chalcopyrites: Structure, Magnetism and Optical Properties. *Materials Chemistry and Physics*, 136(2–3):415–423, 2012.

- [18] J. Yao, C.D. Brunetta, and J.A. Aitken. Suppression of Antiferromagnetic Interactions Through Cu Vacancies in Mn-Substituted CuInSe<sub>2</sub> Chalcopyrites. *Journal of Physics: Condensed Matter*, 24(8):086006, 2012.
- [19] J. Yao, C.N. Kline, H. Gu, M. Yan, and J.A. Aitken. Effects of Mn Substitution on the Structure and Properties of Chalcopyrite-Type CuInS<sub>2</sub>. *Journal of Solid State Chemistry*, 182(9):2579–2586, 2009.
- [20] R.V. Demin, L.I. Koroleva, S.F. Marenkin, V.M. Novotortsev, B.M. Trukhan, S.A. Varnavskii, T.G. Aminov, G.G. Shabunina, R. Szymczak, and M. Baran. Heterogeneous Magnetic State in Mn-doped CdGeP<sub>2</sub> and CuGaTe<sub>2</sub>. In N. Perov, editor, *Proceedings The third Moscow International Symposium on Magnetism*, pages 24–27, Moscow, June 2005. Moscow State University, Elsevier.
- [21] S. Schorr, R. Hoehne, D. Spemann, Th. Doering, and B.V. Korzun. Magnetic Properties Investigations of Mn Substituted ABX<sub>2</sub> Chalcopyrites. *Physica Status Solidi (A)*, 203(11):2783–2787, 2006.
- [22] V.M. Novotortsev, G.G. Shabuninab, L.I. Koroleva, T.G. Aminov, R.V. Demin, and S.V. Boichuk. Superparamagnetism in Mn-doped CuGaTe<sub>2</sub>. *Inorganic Materials*, 43(1):12–17, 2007.
- [23] S. Torres-C., P. Grima-G., M. Muñoz, S. Durán, M. Quintero, L. Nieves, and R. Tovar. Magnetic Behavior of the Alloy (CuInSe<sub>2</sub>)<sub>1-x</sub>(FeSe)<sub>x</sub> with  $x = 0.5$ . *Acta Científica Venezolana*, 66(1):56–59, 2015.
- [24] P. Grima-G., E. Calderón, M. Muñoz-P., S. Durán-P., M. Quintero, E. Quintero, M. Morcoima, G.E. Delgado, H. Romero, Briceño J.M., and J. Fernández. Synthesis and Characterization of Cu<sub>3</sub>TaIn<sub>3</sub>Se<sub>7</sub> and CuTa<sub>2</sub>InTe<sub>4</sub>. *Physica Status Solidi (A)*, 205(7):1552–1559, 2008.
- [25] Y.-J. Zhao and A. Zunger. Electronic Structure and Ferromagnetism of Mn-Substituted CuAlS<sub>2</sub>, CuGaS<sub>2</sub>, CuInS<sub>2</sub>, CuGaSe<sub>2</sub> and CuGaTe<sub>2</sub>. *Physical Review B*, 69:104422, 2004.
- [26] Y.-J. Zhao and A. Zunger. Site Preference for Mn Substitution in Spintronic CuM<sup>III</sup>X<sup>VI</sup><sub>2</sub> Chalcopyrite Semiconductors. *Physical Review B*, 69:075208, 2004.
- [27] A.V. Kochura, S.V. Ivanenko, A. Lashkul, E.P. Kochura, S.F. Marenkin, I.V. Fedorchenko, A.P. Kuzmenko, and E. J. Lahderanta. Magnetic Properties of A<sup>II</sup>B<sup>IV</sup>C<sup>V</sup><sub>2</sub> Compounds Doped with Mn. *Nano and Electronic Physics*, 5(4):04013(1)–04013(4), 2013.
- [28] L. Kilanski, W. Dobrowolski, R. Szymczak, E. Dynowska, M. Wójcik, N. Romcevic, I.V. Fedorchenko, and S.F. Marenkin. Chalcopyrite Semimagnetic Semiconductors: From Nanocomposite to Homogeneous Material. *Science of Sintering*, 46(3):271–281, 2014.
- [29] J.A. Aitken, G.M. Tsoi, L.E. Wenger, and S.L. Brock. Emergence of Pressure-Induced Metamagnetic-Like State in Mn-doped CdGeAs<sub>2</sub> Chalcopyrite. *Chemistry of Materials*, 83:1809, 2007.
- [30] T. Dietl, H. Ohno, and F. Matsukura. Hole-Mediated Ferromagnetism in Tetrahedrally Coordinated Semiconductors. *Physical Review B*, 63:195205, 2001.
- [31] T. Katamani and H.J. Akai. Magnetic Properties of Chalcopyrite-Based Diluted Magnetic Superconductors. *Journal of Superconductivity*, 16:95–97, 2003.
- [32] T. Katamani and H.J. Akai. The Magnetic Properties in Transition Metal-Doped Chalcopyrite Semiconductors. *Materials Science in Semiconductor Processing*, 6(5–6):389–391, 2003.
- [33] P. Mahadevan and A. Zunger. Room-Temperature Ferromagnetism in Mn-Doped Semiconductors CdGeP<sub>2</sub>. *Physical Review Letters*, 88:159904, 2002.
- [34] H. Akai. Ferromagnetism and its Stability in the Diluted Magnetic Semiconductor (In, Mn)As. *Physical Review Letters*, 81:3002, 1998.



- [35] D. Dietl. Origin of Ferromagnetic Response in Diluted Magnetic Semiconductors and Oxides. *Journal of Physics: Condensed Matter*, 19(33):(165204)1–15, 2007.
- [36] P. Grima-G., M. Muñoz-P., S. Durán-P., M. Quintero, G.E. Delgado, J.M. Briceño, H. Romero, J. Ruiz, and J. Fernández. Preparation and Investigation of  $(\text{CuInSe}_2)_{1-x}(\text{TaSe})_x$  Solid Solutions ( $0 < x < 0.5$ ). *Revista Mexicana de Física*, S 53:260–262, 2007.
- [37] P. Grima-G., M. Muñoz-P., S. Durán-P., G.E. Delgado, M. Quintero, and J. Ruiz. Preparation and Investigation of the Quaternary Alloy  $\text{CuTaInSe}_3$ . *Materials Research Bulletin*, 42:2067–2071, 2007.
- [38] G.E. Delgado, A.J. Mora, P. Grima-G., S. Durán, M. Muñoz, and M. Quintero. Crystal Structure of the Quaternary Alloy  $\text{CuTaInSe}_3$ . *Crystal Research & Technology*, 43(7):783–785, 2008.
- [39] P. Grima-G., E. Calderón, M. Muñoz-P., S. Durán-P., M. Quintero, E. Quintero, M. Morocoima, G.E. Delgado, H. Romero, J.M. Briceño, and J. Fernández. Synthesis and Characterization of  $\text{Cu}_3\text{TaIn}_3\text{Se}_7$  and  $\text{CuTa}_2\text{InTe}_4$ . *Physica Status Solidi (A)*, 205(7):1552–1559, 2008.
- [40] C.S. Sunandana, K Chandrasekaran, G. Aravamudan, and G.V. Subba-R. Electrical Properties of  $\text{In}_x\text{MCh}_2$  ( $\text{M} \equiv \text{Nb, Ta}$ ;  $\text{Ch} \equiv \text{S, Se}$ ). *Journal of Less-Common Metals*, 84:115–118, 1982.
- [41] P. Pyykkö and M. Atsumi. Molecular Single-Bond Covalent Radii for Elements 1–118. *Chemistry – A European Journal*, 15(1):187–197, 2009.
- [42] G.E. Delgado, A.J. Mora, P. Grima-G., and M. Quintero. Crystal Structure of  $\text{CuFe}_2\text{InSe}_4$  from X-ray Powder Diffraction. *Journal of Alloys Compounds*, 454:306–409, 2008.
- [43] P. Grima-G., S. Torres, M. Quintero, L. Nieves, E. Moreno, and G.E. Delgado. Phase Diagram of  $\text{CuFe}_2\text{InSe}_4$  Alloys. *Journal of Alloys Compounds*, 630:146–150, 2015.

### Author affiliations

- <sup>1</sup>Centro de Estudios en Semiconductores, Departamento de Física, Facultad de Ciencias,  
Universidad de Los Andes, Mérida, Venezuela
- <sup>2</sup>Centro Nacional de Tecnologías Ópticas, Mérida, Venezuela
- <sup>3</sup>Centro de Investigaciones de Astronomía, Mérida, Venezuela
- <sup>4</sup>Laboratorio de Cristalografía, Departamento de Química, Facultad de Ciencias, Universidad de Los Andes,  
Mérida, Venezuela
- <sup>5</sup>Instituto de Ciencia y Tecnología de Materiales, Universidad de La Habana, Vedado, Cuba
- <sup>6</sup>Instituto Politécnico Nacional. Centro de Investigación en Ciencia Aplicada y Tecnología Avanzada, Unidad  
Legaria,  
México D.F, México
- <sup>7</sup>Dept. of Chemistry and Biochemistry, Duquesne University, Pittsburgh, USA
- <sup>8</sup>Dept. of Physics, Pachhunga University College, Aizawl, India

